Research Article

Received: 19 November 2015 Revised: 14 March 2016 Accepted article published: 4 May 2016 Published online in Wiley Online Library: 31 May 2016

(wileyonlinelibrary.com) DOI 10.1002/pi.5150

Development and characterization of bionanocomposites based on poly(3-hydroxybutyrate) and cellulose nanocrystals for packaging applications

Irene T Seoane,[a] Elena Fortunati,[b] Debora Puglia,[b] Viviana P Cyras[a] and Liliana B Manfredi[a]*

Abstract

Poly(3-hydroxybutyrate) (PHB)-based bionanocomposites were prepared using various percentages of cellulose nanocrystals (CNCs) by a solution casting method. CNCs were prepared from microcrystalline cellulose using sulfuric acid hydrolysis. The influence of CNCs on PHB properties was evaluated using differential scanning calorimetry, Fourier transform infrared spectroscopy, X-ray diffraction, thermogravimetry and tensile testing. Vapor permeation and light transmission of the materials were also measured. Differential scanning calorimetric tests demonstrated that CNCs were effective PHB nucleation agents. Tensile strength and Young's modulus of PHB increased with increasing CNC concentration. Moreover, the PHB/CNC bionanocomposites exhibited reduced water vapor permeation compared to neat PHB and had better UV barrier properties than commodity polymers such as polypropylene. It was found that nanocomposites with 6 wt% of CNCs had the optimum balance among thermal, mechanical and barrier properties.

Keywords: cellulose nanocrystals; poly(3-hydroxybutyrate); biodegradable polymers; nanocomposites

INTRODUCTION

Biopolymers derived from renewable resources have attracted widespread attention due to the disposal problems at the end of life for synthetic and petroleum-based polymers. Polyhydroxyalkanoates (PHAs), biopolyesters biosynthesized by microorganisms, are a promising alternative to petroleum-based plastics due to their wide range of potential applications.[1] Polyhydroxybutyrate (PHB) is the most common PHA and widely studied due to its good biodegradability and biocompatibility, but its high cost and brittleness limits its applications. Another advantage is that it can be extruded or molded using conventional processing equipment, so it appears as a good candidate for producing biodegradable packaging applicable to food, agricultural and medical fields.[2] Additionally, nowadays there is emerging a great quantity of work dealing with the development of methods to produce PHB from various waste sources,[3,4] which surely will be useful for improving industrial-scale production and lowering costs in a short time. Because of this, it is important to develop new materials based on PHB, maintaining its excellent properties, but improving those that are not as good such as fragility and short processing window. Diverse approaches have been studied with the purpose of improving the mechanical and thermal properties as well as the processing of PHB, including the use of copolymers,[5] the addition of a different polymer to obtain blends[6–8] or the preparation of nanocomposites with nanofillers.[9,10] In general, blending or preparation of composites is easier and faster than copolymerization methods. Blend or nanocomposite properties depend on composition, chemical or physical interaction of the components, processing conditions, final morphology and crystallization behavior of PHB. Thus, the preparation of nanocomposites could be promising to achieve improvement in the properties of PHB. In this context, cellulose derivatives are optimal reinforcing materials for the bioplastic industry since they are bio-based, biodegradable, stiff, lightweight, non-abrasive to the processing equipment and highly abundant in nature at low cost.[11–13] Nanocellulose shows a great variety of advantages such as extraordinary mechanical properties, reinforcing capabilities, low density, abundance and biodegradability.[14]

Several biodegradable polymers such as poly(lactic acid) (PLA),[15–17] polycaprolactone,[18] PHAs[19] and PLA/PHB blends[20,21] have been used as matrices for nanocellulose reinforcement. Particularly, several works were aimed at studying the effect of nanocellulose addition on the properties of

* *Correspondence to: LB Manfredi, Instituto de Investigaciones en Ciencia y Tecnología de Materiales (INTEMA), UNMdP, CONICET, Facultad de Ingeniería, Av. Juan B Justo 4302, B7608FDQ Mar del Plata, Argentina. E-mail: lbmanfre@fi.mdp.edu.ar*

a *Instituto de Investigaciones en Ciencia y Tecnología de Materiales (INTEMA), UNMdP, CONICET, Facultad de Ingeniería, Av. Juan B Justo 4302, B7608FDQ, Mar del Plata, Argentina*

b *University of Perugia, Civil and Environmental Engineering Department, UdR INSTM Strada di Pentima 4, 05100, Terni, Italy*

poly[(3-hydroxybutyrate)-*co*-(3-hydroxyvalerate)] (PHBV), which is the most widely studied PHB copolymer.[22–25] It was reported that the nanoparticles increased the tensile strength, Young's modulus and storage modulus of PHBV, and also acted as nucleating agent. Additionally, to the best of our knowledge, there have been few works concerning PHB and nanocellulose composites.[26–28] Dhar *et al.*[26,27] focused their study on the thermal degradation kinetics as well as on the migration and barrier properties of PHB/cellulose nanocrystal (CNC) nanobiocomposites. They concluded that PHB thermal stability was improved up to 3 wt% of CNC loading but with no significant change in activation energies nor in degradation mechanism. On the other hand, migration studies on PHB/CNC films in two food simulants provided values within standard limits, and the oxygen transmission rate decreases significantly even at low CNC (*ca* 2 wt%) loadings. Meanwhile Patrício *et al.*[28] obtained nanocomposites by dispersing the nanocellulose in poly(ethylene glycol) plasticizer prior to incorporation in PHB. They found an enlargement in the processing window of the nanocomposites in comparison to the neat PHB and a marked increase in the strain level without a significant loss of the tensile strength with the incorporation up to 0.45 wt% of nanocellulose.

Thus, the aim of the research presented here was to study the overall impact of CNCs on PHB properties, without plasticizer, evaluating the improvement of the poor properties (such as mechanical properties) as well being non-detrimental to its good ones (such as barrier and transparency). In this context, special emphasis was placed on the permeation of water, protection from light and mechanical properties considering a potential application of this material as food packaging. Moreover, combining bio-based polymers with renewable reinforcements could address the goal of obtaining sustainable green composites with notable properties.

EXPERIMENTAL

Materials

PHB ($M_w = 324\,900$ g mol^{-1}) was kindly supplied by Biocycle®. Microcrystalline cellulose (dimensions of 10–15 µm) was supplied by Sigma-Aldrich (St Louis, MO, USA). *N*,*N*-Dimethylformamide (DMF) and sulfuric acid were from Cicarelli.

Extraction of cellulose nanocrystals

CNCs were extracted by hydrolysis from microcrystalline cellulose in a sulfuric acid solution (64 wt%) at 45 °C with vigorous stirring for 30 min. The resultant CNC aqueous suspension, obtained after centrifugation, dialysis and ultrasonic treatment, was approximately 0.5 wt% and the yield was *ca* 20%.[29] Then, an ion exchange resin (Dowex Marathon MR-3 hydrogen and hydroxide form) was added to the cellulose suspension for 24 h in order to remove all the ionic materials, except H^+. After removing the exchange resin by filtration and to ensure the thermal stability of the CNCs, the pH of the suspension was raised to approximately 9 with a 0.25 wt% NaOH solution. The CNC suspension obtained after the acid hydrolysis was directly cast on to silicon and observed using a field emission SEM instrument (Supra 25-Zeiss) after gold sputtering. Moreover, CNCs were also examined using a transmission electron microscopy (TEM) instrument (Philips Tecnai 10) operated at an acceleration voltage of 80 kV. A droplet of dilute CNC suspension (0.1 wt%) was deposited on a bacitracin-pretreated surface of a carbon-coated grid. Finally, for the preparation of PHB-based bionanocomposites, the obtained CNC solution was freeze-dried in order to obtain cellulose powder.

Preparation of PHB bionanocomposites

Homogeneous solutions of PHB in DMF were prepared by stirring at 116 °C, allowing the complete dissolution of PHB but avoiding its degradation. Various percentages of CNCs (2, 4 and 6 wt%) in a DMF solution previously sonicated for 10 min in an ice-bath were added to the PHB solution and then again sonicated for 10 min. Finally, the mix was poured into Petri dishes and kept in an oven at 80 °C for 12 h to eliminate solvent by evaporation. The films were stored at room temperature for 15 days to allow complete PHB crystallization.

Bionanocomposite characterization

Fourier transform infrared (FTIR) spectra were acquired with a Mattson Genesis II spectrometer, with a spectral width of 400–4000 cm^{-1}, 32 accumulations and a resolution of 4 cm^{-1}. For comparison purposes, the spectra were normalized with the intensity of the band near 2933 cm^{-1}, which corresponds to the CH_2 group that is present in all samples.

XRD patterns were obtained with Cu Kα ($\lambda = 1.54$ Å) radiation using a Philips PW 1710 system. The X-ray tube was operated at 45 kV and 30 mA, at 2° min^{-1} in the 2θ range from 5° to 60°. The percentage of crystallinity (X_c) of the materials was calculated by means of the following equation:

$$X_c\ (\%) = \frac{(\text{total area}) - (\text{amorphous area})}{\text{total area}} \quad (1)$$

Calorimetric analysis was carried out using a PerkinElmer DSC instrument under nitrogen atmosphere. The first heating run was made from ambient temperature to 195 °C, at a rate of 10 °C min^{-1}. Then, the samples were cooled to −50 °C at a rate of 80 °C min^{-1}, and a second heating run was carried out at a rate of 10 °C min^{-1} from −50 to 195 °C.

Dynamic thermal degradation measurements were performed with a TA Instruments Auto-MTGA Q500 Hi-Res thermogravimetric analyzer. Temperature was raised from room temperature to 700 °C at a heating rate of 10 °C min^{-1}. All runs were carried out under nitrogen atmosphere (30 mL min^{-1}) in order to prevent any thermo-oxidative reaction. The sample weight in all tests was approximately 10 mg.

The mechanical properties of the composites were determined with an Instron 4467 mechanical testing machine. Tensile testing of bone-shaped composite specimens was carried out using a crosshead rate of 1 mm min^{-1} (ASTM D 1708–93). SEM of the fractured surfaces, previously coated with a 300 Å gold layer, was performed with a JEOL JSM-6460LV instrument.

Nanoindentation experiments were carried out on films using a Hysitron triboindenter equipped with a scanning probe microscope module. The tests were performed under load control conditions using a diamond Berkovich tip with a maximum load of 9 mN. A holding period of 30 s was applied at maximum load between loading and unloading stages to minimize the creep effect on the unloading curve.[30] Five indentations were made for each sample. Using the approach outlined by Oliver and Pharr, reduced elastic modulus (E_r) and indentation hardness (H) were calculated for each sample.[31]

Water vapor permeability (WVP) tests were conducted according to ASTM E 96-00e1. Each film sample was sealed over a circular opening of 0.00177 m^2 in a permeation cell and was conditioned at 20 °C in desiccators before being analyzed. Test cells were placed in a conditioned chamber at 20 °C and 64.5% of relative humidity (RH). Anhydrous $CaCl_2$ (0% RH) was placed inside the cell

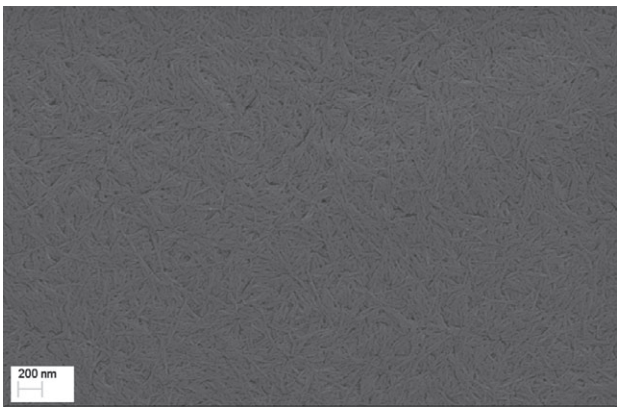

Figure 1. Field emission SEM image of CNCs.

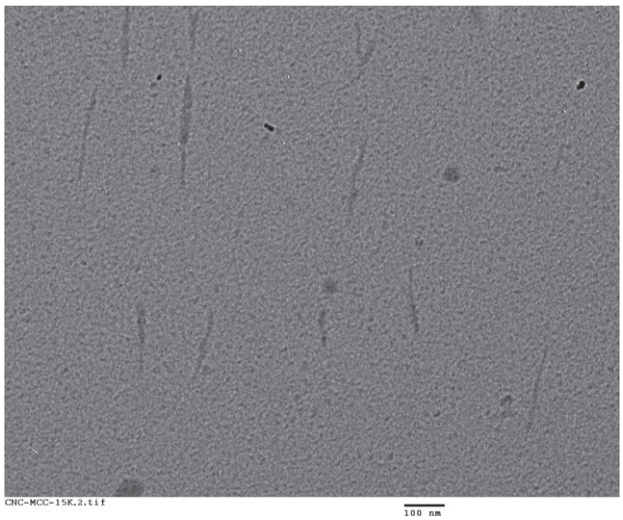

Figure 2. TEM image of CNCs.

to maintain a humidity gradient across the film. The RH inside the cell was always lower than that outside, and water vapor transport was determined from the weight gain of the permeation cell. When steady-state conditions were reached (about a day), weight measurements were made over 10 days. Changes in the weight of the cell were recorded as a function of time for all the samples. Water vapor transmission rate (WVTR) is a weight gain and was calculated as the relation between the slope of each curve of weight *versus* time (g s^{-1}), determined by linear regression, and the cell area (m^2). WVP (g s^{-1} m^{-1} Pa^{-1}) was then calculated according to the following equation:

$$\mathrm{WVP} = \frac{\mathrm{WVTR}}{S\left(R_2 - R_1\right)} \times d \qquad (2)$$

where S is vapor pressure of water at saturation (Pa) at test temperature (20 °C), R_1 is RH inside the permeation cell ($R_1 = 0$), R_2 is RH in the chamber ($R_2 = 64.5\%$) and d is film thickness (m). Each WVP reported was the mean value of at least six samples.

The absorption spectra of nanocomposites, obtained in the 250–700 nm region, were obtained using an Agilent 8453 UV-visible spectrophotometer.

RESULTS AND DISCUSSION

The resulting CNC aqueous suspension from microcrystalline cellulose was of approximately 0.5 wt%, while the hydrolysis yield was *ca* 20%. Field emission SEM (Fig. 1) and TEM (Fig. 2) observations of CNCs showed well individualized crystals with dimensions ranging from 100 to 200 nm in length and 5–10 nm in width, in agreement with previous work.[32]

FTIR spectra of the CNCs, PHB and nanocomposites were acquired in order to characterize the bionanocomposites (Fig. 3). The characteristic bands of CNC appear in the 800–1400 and 3000–3500 cm^{-1} regions. The peaks at 1061 and 897 cm^{-1} correspond to C—O stretching and C—H rocking vibrations of cellulose, the small band at 895 cm^{-1} is due to glycosidic —C1—H deformation, with a ring vibration contribution and —OH bending, and the band at 1428 cm^{-1} is assigned to —CH_2— bending. The broad peak at 3342 cm^{-1} is characteristic of the stretching vibration of O—H.[33] Additionally, the signals at 1428, 1163, 1113, and 897 cm^{-1} indicate that the CNCs are predominantly in the form of cellulose I.[34]

The PHB characteristic bands correspond to the C—O—C bond (1279, 1228 and 1185 cm^{-1}) and the C═O bond (1722 and 1740 cm^{-1}). The signals at 1279 and 1722 cm^{-1} are more intense in the crystalline state, while in the amorphous state those at 1185 and 1740 cm^{-1} become predominant.[35]

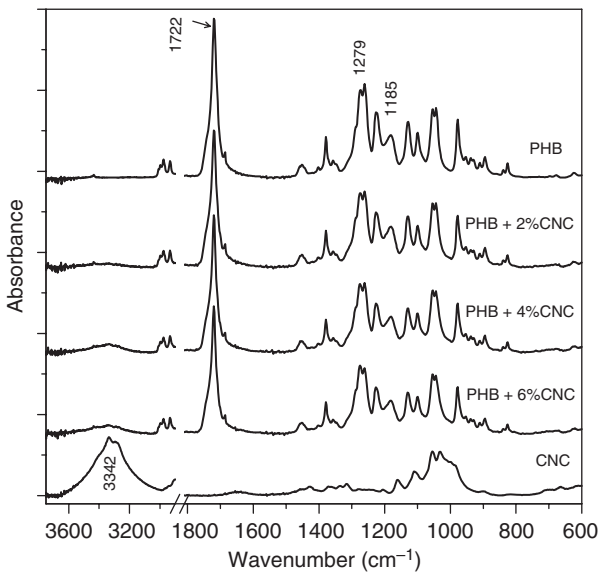

Figure 3. FTIR spectra of CNCs, PHB and nanocomposites.

It is observed that the typical bands of PHB in the FTIR spectra are not modified by the addition of nanocellulose crystals. Furthermore, the range 1650–1700 cm^{-1} due to the stretching vibration of carbonyl is broader with CNC content. This is consistent with the appearance of another band at 1709 cm^{-1} related to the hydrogen interactions between the C═O groups in PHB and —OH groups in CNC, as reported by Patrício *et al.*[28] Moreover, the presence of CNCs in the bionanocomposites could also be observed in the 3000–3500 cm^{-1} region due to the presence of a broad band which became stronger with the increase of cellulose content in the films.

The percentage crystallinity of the PHB and bionanocomposite films was calculated from the XRD analysis (Fig. 4) according to Eqn (1) and the results are summarized in Table 1. It is observed that X_c of the PHB films is equal to 66.1% and it slightly increases

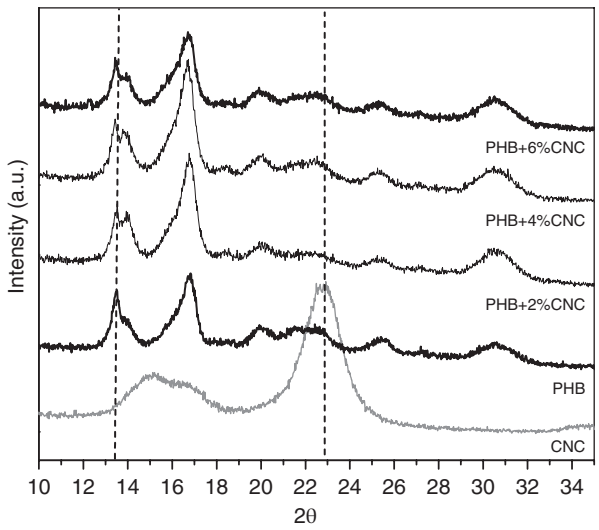

Figure 4. XRD spectra of PHB, CNCs and nanocomposites with 2, 4 and 6 wt% of CNCs.

Table 1. Percentage crystallinity (X_c) of PHB-based bionanocomposites

Material	X_c (%)		
	XRD	DSC (first heating)	DSC (cooling)
PHB	66.1	55.0	25.5
PHB + 2 wt% CNCs	69.7	55.4	43.1
PHB + 4 wt% CNCs	69.3	55.3	42.8
PHB + 6 wt% CNCs	68.5	55.8	44.1

with CNC addition, because of the crystalline nature of CNCs. Moreover, the CNC addition does not significantly modify the crystalline structure of PHB.[36] Typical PHB peaks corresponding to the planes (0 2 0), (1 1 0) and (1 1 1) appear at $2\theta = 13.5°$, 16.8° and 22.3°, respectively.[37] On the other hand, CNCs exhibit four main reflection peaks at $2\theta = 15.0°$, 16.3°, 22.7° and 34.4° (less defined) relative to the cellulose I crystalline structure.[17] The appearance of the CNC peaks and little changes in the form of the characteristic peaks of crystalline planes of PHB are observed in the nanocomposite spectra (Fig. 4). Particularly, a slight displacement to lower angles of the peak at 13.5° with CNC content is observed, probably due to CNC intercalation through hydrogen bonding interaction with the ester groups of PHB.[26] Besides, the peak at 22.7° shows a broadening in the nanocomposite spectra compared to PHB due to the presence of CNCs, because it is the strongest peak characteristic of cellulose I.

The great importance of the knowledge of the crystallization and melting behavior of polymeric materials is because it could affect not only their morphology and crystalline structure but also their final properties. Figure 5(a) shows the thermograms corresponding to the first heating on DSC of PHB and nanocomposites. Observed are two characteristic melting peaks of PHB in all of the samples demonstrating a melting–recrystallization–remelting process. The lower temperature melting peak (T_{m1}) is attributed to the melting of original crystals formed during the casting process, before the DSC scan, and the higher one (T_{m2}) is associated with the melting of the recrystallized crystals during the heating scan.[38] A slight displacement of the first peak of the

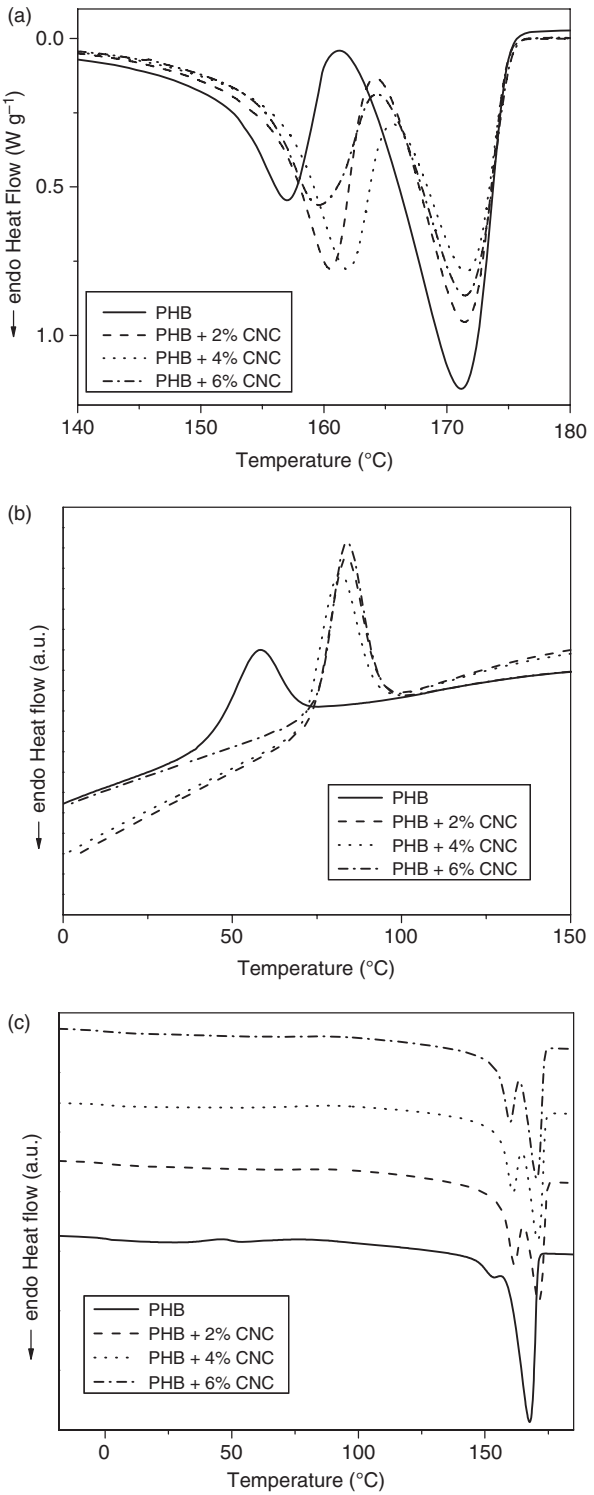

Figure 5. DSC scans of PHB and its composites with CNCs: (a) first heating; (b) cooling; (c) second heating.

bionanocomposites to higher temperatures is observed, independent of the percentage of CNCs added. This indicates that the cellulose nanostructures facilitate PHB crystal growth leading to larger lamellar thickness of the spherulites during the casting process, which consequently leads to increased melting points, but without significantly modifying the PHB crystallinity (Table 1).

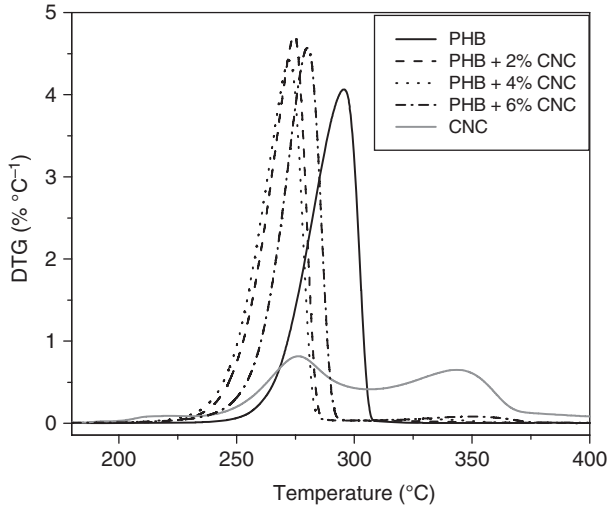

Figure 6. DTG curves of PHB, CNC and nanocomposites.

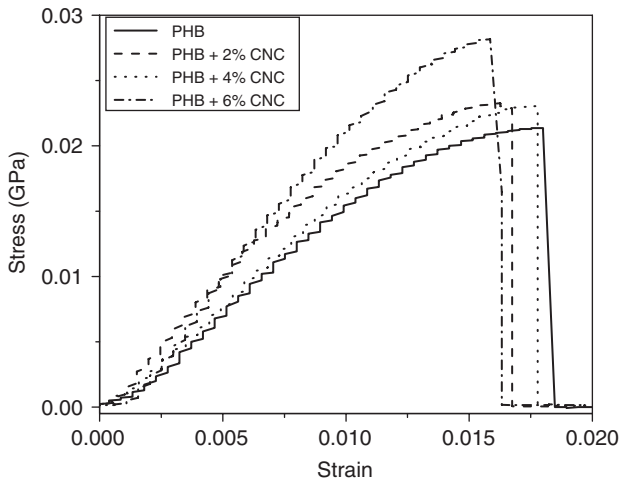

Figure 7. Stress–strain curves of materials from the tensile tests.

The DSC scans of the cooling process at 10 °C min^{-1} (Fig. 5(b)) reveal that CNCs act as effective nucleation agents reducing the energy barrier to form PHB nuclei. Clearly seen is an exothermic peak at approximately 83 °C, which is similar for all the nanocomposites and shifts to lower temperature for pristine PHB. The percentage crystallinity of PHB calculated in the pristine film and in the nanocomposites from the DSC curves (Table 1) is similar for all the materials. Then, the CNCs favor the crystallization of PHB but without significantly changing the percentage crystallinity. A similar nucleation behavior of CNCs was previously found for nanocomposite formulations based on biodegradable polymers such as PLA[39] or PHBV.[24]

The crystallization peak of PHB is not observable during the second heating scan of the materials (Fig. 5(c)) because it already crystallized during cooling. Moreover, the magnitude of T_{m2} in area relative to that of T_{m1} becomes larger in the second heating scan than in the first one. It seems that the crystals formed from the melt are more imperfect than those formed during casting, so they will recrystallize and reorganize into more perfect and stable crystals during the subsequent heating scans.[40]

Thermal analyses were conducted in order to study the effect of CNC addition on the thermal stability of the polymer matrix. The first derivative of the weight loss curve with respect to temperature (DTG) from TGA tests of the materials is shown in Fig. 6. The peak of the first derivative indicates the point of greatest rate of change on the weight loss curve. It can be observed that the PHB degrades in a single step showing the maximum of the peak of the DTG curve at 295 °C. On the other hand, CNCs start to degrade at lower temperature than PHB, showing two main

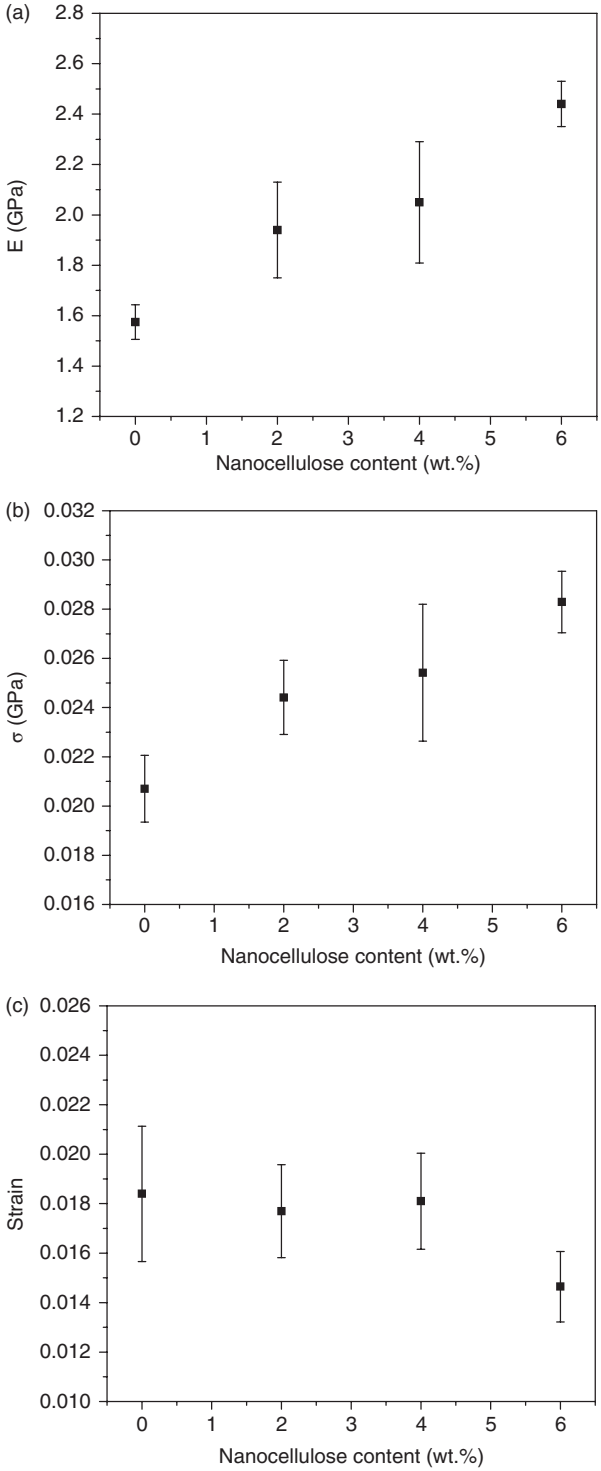

Figure 8. Effect of nanocellulose content on mechanical properties of PHB/CNC nanocomposites: (a) Young's modulus; (b) tensile strength; (c) elongation at break.

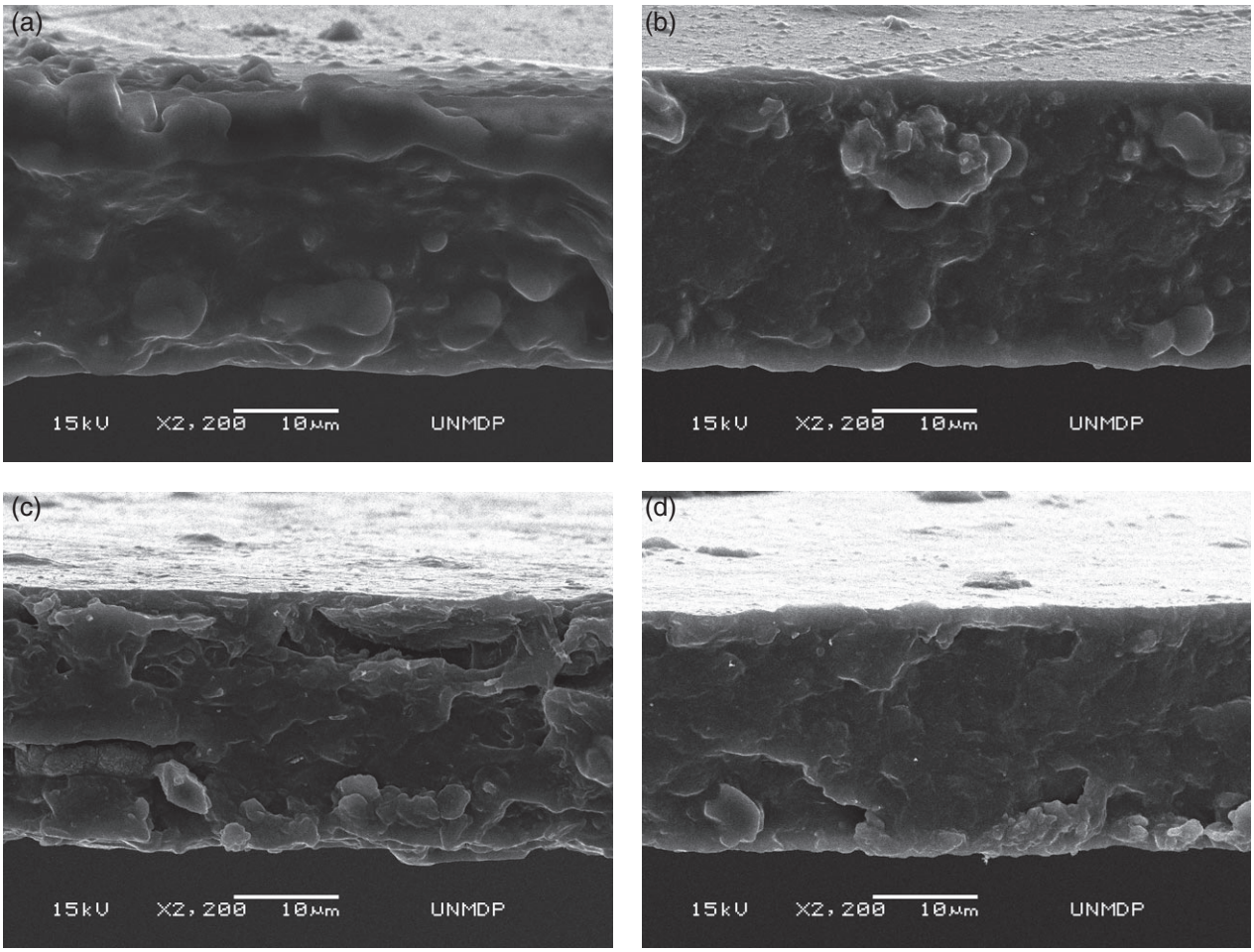

Figure 9. SEM images of fractured surfaces of (a) PHB, and nanocomposites with (b) 2 wt%, (c) 4 wt% and (d) 6 wt% of CNCs.

peaks: the first one is attributed to the introduction of sulfate groups via microcellulose sulfuric acid hydrolysis.[41] In detail, DTG thermograms show that all materials are thermally stable up to 200 °C; however, the bionanocomposites show a 20 °C lower thermal resistance than PHB, which is slightly improved with the percentage of CNCs added. This shows that CNCs have a synergistic effect on degradation of PHB, due to the presence of pendant sulfate and hydroxyl groups on CNC surface which act as nucleation sites for the chain scission of PHB at higher temperature.[21,26]

The mechanical response of PHB-based formulations reinforced with various contents of CNCs was investigated by tensile testing and typical curves are shown in Fig. 7. It is observed that a low fraction of CNCs has an appreciable effect on PHB mechanical properties. The tensile modulus and strength of PHB are enhanced with an increase in CNC content (Figs 8(a) and (b)). Those properties are improved with an increase of 50 and 35%, respectively, with the addition of 6 wt% of CNCs. On the other hand, the elongation at break is slightly reduced (Fig. 8(c)). This behavior could be attributed to the restrained chain movement during the deformation due to the presence of the nanocellulose. Similar results were reported for nanocellulose-based nanocomposites with PHB and PHBV matrices.[42] The fractured surfaces of the films after the tensile test were investigated by means of SEM in order to investigate the dispersion of CNCs in the polymeric matrix. Figure 9 shows micrographs of neat PHB and the nanocomposites, where a certain rougher surface is observed in all the samples. Nanocellulose can be detected as white dots in the nanocomposites, which are clearly seen in the samples with 4 and 6 wt% of CNCs (Figs 9(c) and (d)), showing a homogeneous dispersion.

The reduced elastic modulus (E_r) was also obtained using the nanoindentation technique. This technique obtains the elastic and hardness features of small volumes of material of thin films by performing indentations at very low loads.[43] E_r and hardness values obtained for each film are shown in Fig. 10. The highest modulus is found for the PHB film containing 2 wt% of CNCs, indicating that the reinforcement effect of the CNCs in PHB matrix plays an important role in the tensile deformation even at low concentration; indeed the modulus leveled at the same value with increasing CNC content. The decrease in E_r upon addition of 4 and 6 wt% CNCs suggests that the CNCs might be creating weak interfaces between the nanocomposite domains. The nanoindentation hardness results reveal similar average results with slightly or unappreciable differences between samples, with values in the range of 155–165 MPa. *H* slightly increases upon addition of CNCs, suggesting good CNC–matrix interactions at the surface.[44]

Figure 11 shows the effect of different amounts of CNCs on the WVP of PHB. It is observed that the addition of CNCs reduces the permeation of the PHB despite the hydrophilic character of the nanoparticles.[45] In general, a comparable improvement in the WVP for all the nanocomposite formulation is found compared with PHB. This result is an effect of the tortuous pathway for the

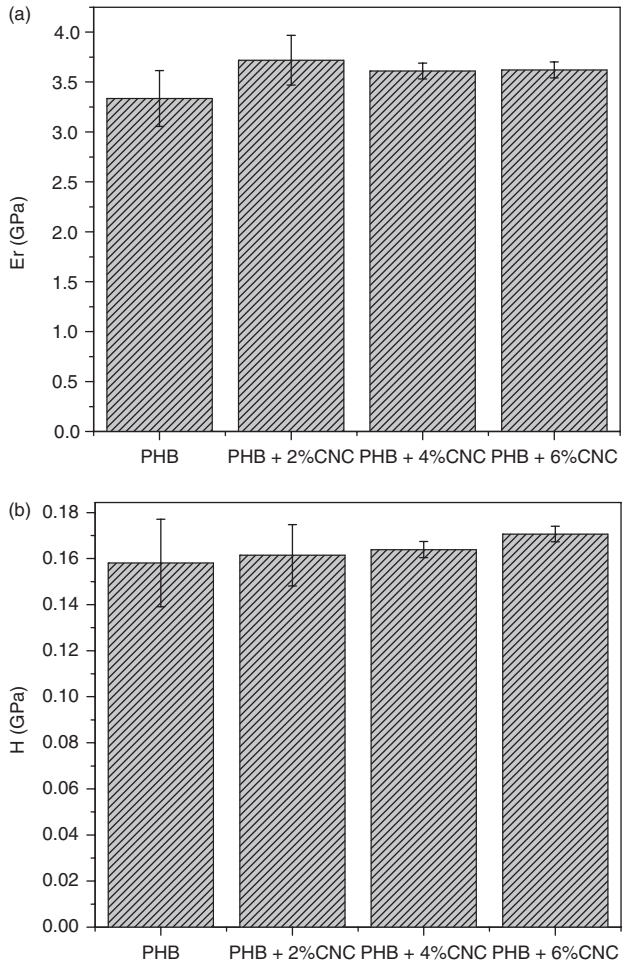

Figure 10. Nanoindentation results: (a) reduced elastic modulus; (b) hardness.

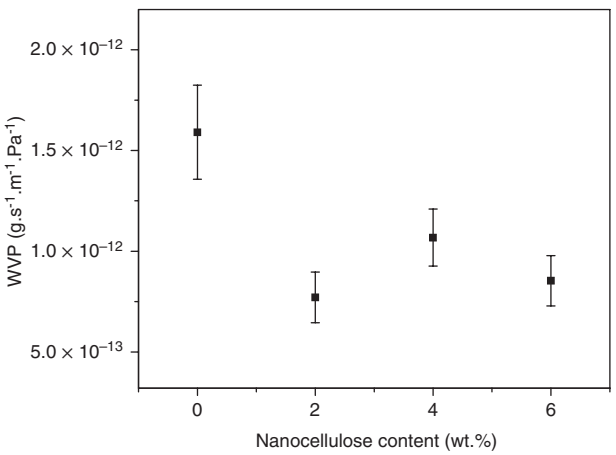

Figure 11. WVP of PHB and nanocomposites.

vapor induced by the nanofillers which act as physical barriers forcing the water molecules to wiggle around them.[46] Additionally, it has been reported that the tortuosity depends on a number of factors such as shape and aspect ratio of filler, filler loading and orientation, degree of exfoliation or dispersion, adhesion to the matrix, polymer chain immobilization and porosity, among others.[47]

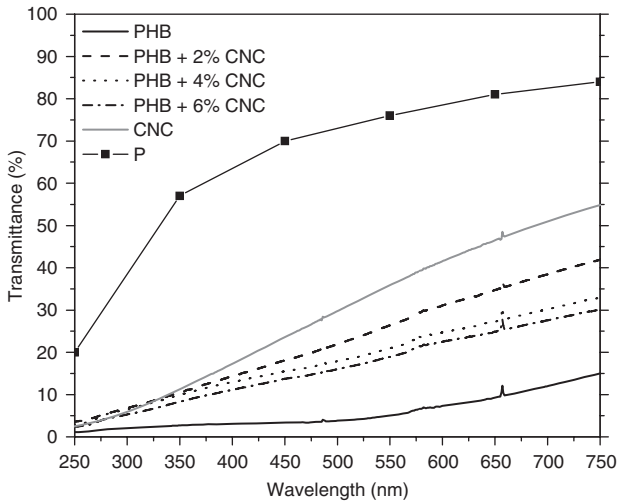

Figure 12. UV-visible spectra of PHB, CNCs and nanocomposites, and polypropylene (PP).

Light protection is a basic requirement for a packaging system of food products and the development of a transparent material with enhanced UV protection is especially useful. Film transparency of the PHB-based bionanocomposites was determined using UV-visible spectroscopy and the spectra are shown in Fig. 12. CNC-based films present the highest UV-visible transmission. Nanocomposite films show behavior intermediate between that of PHB and CNC films. This could be attributed to the homogeneous dispersion of the nanoparticles and to the good interaction between CNC and PHB, thus reducing the amount of light scattering and favoring the transmittance of visible light through the films. At high-energy range (220 to 400 nm) nanocomposites have low transmission, up to 10%, in accordance with the reduced transmittance of the components at this radiation range. This result indicates that nanocomposites have better UV barrier properties than commodity polymers such as polypropylene, which presents 40 to 60% transmittance at the same radiation range, as included in Fig. 12.[48]

CONCLUSIONS

It was possible to obtain via solution casting homogeneous films of PHB with various nanocellulose contents from 2 to 6 wt%. The presence of CNCs in the bionanocomposites was corroborated by FTIR and XRD analyses, due to the appearance of characteristic peaks. From the DSC thermograms of the first heating scan was observed the melting–recrystallization–remelting behavior of PHB as well as evidences of a larger lamellar thickness of the spherulites in the nanocomposites due to the displacement of the first peak of fusion to higher temperatures. Additionally, a noticeable nucleating effect of the nanocellulose was found reducing the energy barrier to form PHB nuclei during the cooling DSC scan. CNC addition slightly reduced the thermal degradation resistance of PHB because of the lower degradation temperature of the nanoparticles; however, all the materials were thermally stable up to 200 °C. The reinforcing effect of the nanocellulose was confirmed by the mechanical properties and the WVP which were appreciably enhanced with nanoparticle addition. With 6 wt% of CNCs, the film showed 50% improvement in Young's modulus and 35% increase in tensile strength. The barrier property of PHB in terms of WVP was found to be improved in the nanocomposites

due to the tortuous pathway for the water vapor. It was found that nanocomposites have better UV barrier properties than commodity polymers such as polypropylene. Among the nanocomposites studied, the optimum balance among thermal, mechanical and barrier properties was obtained at a CNC concentration of 6 wt%.

ACKNOWLEDGEMENTS

The authors are grateful to the National Research Council of Argentina (CONICET), International Cooperation Project CNR-CONICET n° 1010, PIP 0014 and 0527, the National Agency of Scientific and Technological Promotion of Argentina (PICT'12 1983), and the National University of Mar del Plata for the financial funding of this research.

REFERENCES

1 Reddy MM, Vivekanandhana S, Misra M, Bhatia SK and Mohanty AK, *Prog Polym Sci* **38**:1653–1689 (2013).
2 Mekonnen T, Mussone P, Khalilb H and Bressler DJ, *Mater Chem A* **1**:13379–13398 (2013).
3 Rahman A, Anthony RJ, Sathish A, Sims RC and Miller CD, *Bioresour Technol* **156**:364–367 (2014).
4 Cavaillé L, Grousseau E, Pocquet M, Lepeuple A-S, Uribelarrea J-L, Hernandez-Raquet G *et al.*, *Bioresour Technol* **149**:301–309 (2013).
5 Chen LJ and Wang M, *Biomaterials* **23**:2631–2639 (2002).
6 Abdelwahab MA, Flynn A, Chiou B-S, Imam S, Orts W and Chiellini E, *Polym Degrad Stab* **97**:1822–1828 (2012).
7 Arrieta MP, López J, Rayón E and Jiménez A, *Polym Degrad Stab* **108**:307–318 (2014).
8 D'Amico DA, Iglesias Montes ML, Manfredi LB and Cyras VP, *Polym Test* **49**:22–28 (2016).
9 Angelini S, Cerruti P, Immirzi B, Scarinzi G and Malinconico M, *Eur Polym J* **76**:63–76 (2016).
10 Tănase EE, Popa ME, Râpă M and Popa O, *Agric Agric Sci Procedia* **6**:608–615 (2015).
11 Brinchi L, Cotana F, Fortunati E and Kenny JM, *Carbohydr Polym* **94**:154–169 (2013).
12 Frone AN, Berlioz S, Chailan J-F and Panaitescu DM, *Carbohydr Polym* **91**:377–384 (2013).
13 Rayón E, Ferrandiz S, Rico MI, López J and Arrieta MP, *Int J Food Prop* **18**:1211–1222 (2014).
14 Moon RJ, Martini A, Nairn J, Simonsen J and Youngblood J, *Chem Soc Rev* **40**:3941–3994 (2011).
15 Fortunati E, Luzi F, Puglia D, Dominici F, Santulli C, Kenny JM *et al.*, *Eur Polym J* **56**:77–91 (2014).
16 Fortunati E, Peltzer M, Armentano I, Jiménez A and Kenny JM, *J Food Eng* **118**:117–124 (2013).
17 Fortunati E, Peltzer M, Armentano I, Torre L, Jiménez A and Kenny JM, *Carbohydr Polym* **90**:948–956 (2012).
18 Siqueira G, Bras J and Dufresne A, *Biomacromolecules* **10**:425–432 (2009).
19 Dufresne A, Kellerhals M and Witholt B, *Macromolecules* **32**:7396–401 (1999).
20 Arrieta MP, Fortunati E, Dominici F, López J and Kenny JM, *Carbohydr Polym* **121**:265–275 (2015).
21 Arrieta MP, Fortunati E, Dominici F, Rayón E, López J and Kenny JM, *Carbohydr Polym* **107**:16–24 (2014).
22 Avella M, Martuscelli E and Raimo M, *J Mater Sci* **35**:523–545 (2000).
23 Ten E, Jiang L, Bahr DF, Li B and Wolcott, MP, *Ind Eng Chem Res* **51**:2941–2951 (2012).
24 Ten E, Turtle J, Bahr D, Jiang L and Wolcott M, *Polymer* **51**:2652–2660 (2010).
25 Jiang L, Morelius E, Zhang J, Wolcott MP and Holbery J, *J Compos Mater* **42**:2629–2645 (2008).
26 Dhar P, Vangala SPK, Tiwari P, Kumar A and Katiyar V, *J Thermodyn Catal* **5**:134 (2014).
27 Dhar P, Bhardwaj U, Kumar A and Katiyar V, *Polym Eng Sci* **55**:2388–2395 (2015).
28 Patrício PSO, Pereira FV, Santos MC, Souza PP, Roa JPB and Orefice RL, *J Appl Polym Sci* **127**:3613–3621 (2012).
29 Fortunati E, Armentano I, Zhou Q, Iannoni A, Saino E, Visai L *et al.*, *Carbohydr Polym* **87**:1596–1605 (2012).
30 Geng K, Yang F, Druffel T and Grulke EA, *Polymer* **46**:11768–11772 (2005).
31 Oliver WC and Pharr GM, *J Mater Res* **7**:1562–1584 (1992).
32 Fortunati E, Puglia D, Luzi F, Santulli C, Kenny JM and Torre L, *Carbohydr Polym* **97**:825–836 (2013).
33 Alemdar A and Sain M, *Bioresour Technol* **99**:1664–1671 (2008).
34 Leung ACW, Hrapovic S, Lam E, Liu Y, Male KB, Mahmoud KA *et al.*, *Small* **7**:302–305 (2011).
35 Cyras VP, Galego Fernández N and Vázquez A, *Polym Int* **48**:705–712 (1999).
36 D'Amico DA, Manfredi LB and Cyras VP, *J Appl Polym Sci* **123**:200–208 (2012).
37 Ten E, Jiang L and Wolcott MP, *Carbohydr Polym* **90**:541–550 (2012).
38 Gunaratne LMWK and Shanks RA, *Eur Polym J* **41**:2980–2988 (2005).
39 Fortunati E, Armentano I, Zhou Q, Puglia D, Terenzi A, Berglund LA *et al.*, *Polym Degrad Stab* **97**:2027–2036 (2012).
40 Xu C and Qui Z, *J Polym Sci B* **47**:2238–2246 (2009).
41 Roman M and Winter WT, *Biomacromolecules* **5**:1671–1677 (2004).
42 de Carvalho KCC, Montoro SR, Cioffi MOH and Voorwald HJC, Polyhydroxyalkanoates and their nanobiocomposites with cellulose nanocrystals, in *Design and Applications of Nanostructured Polymer Blends and Nanocomposite Systems*. Elsevier, Oxford, pp. 261–285 (2016).
43 Roa JJ, Rayon E, Morales M and Segarra M, *Recent Pat Nanotechnol* **6**:142–152 (2012).
44 Ago M, Jakes JE and Rojas OJ, *ACS Appl Mater Interfaces* **5**:11768–11776 (2013).
45 Song Z, Xiao H and Zhao Y, *Carbohydr Polym* **111**:442–448 (2014).
46 Ray SS and Okamoto M, *Prog Polym Sci* **28**:1539–1641 (2003).
47 Sanchez-Garcia MD, Gimenez E and Lagaron JM, *Carbohydr Polym* **71**:235–244 (2008).
48 Bucci DZ, Tavares LBB and Sell I, *Polym Test* **26**:908–915 (2007).

